Coupled Systems Mechanics, *Vol. 12, No. 3 (2023) 277-295*
https://doi.org/10.12989/csm.2023.12.3.277

Mitigation of seismic pounding between two L-shape in plan high-rise buildings considering SSI effect

Ahmed Abdelraheem Farghaly*[1] and Denise-Penelope N. Kontoni**[2,3]

[1]*Department of Civil and Architectural Constructions, Faculty of Technology and Education, Sohag University, Sohag, 82524, Egypt*
[2]*Department of Civil Engineering, School of Engineering, University of the Peloponnese, GR-26334 Patras, Greece*
[3]*School of Science and Technology, Hellenic Open University, GR-26335 Patras, Greece*

(Received March 23, 2022, Revised June 3, 2023, Accepted June 12, 2023)

Abstract. Unsymmetrical high-rise buildings (HRBs) subjected to earthquake represent a difficult challenge to structural engineering, especially taking into consideration the effect of soil-structure interaction (SSI). L-shape in plan HRBs suffer from big straining actions when are subjected to an earthquake (in *x*- or *y*-direction, or both *x*- and *y*- directions). Additionally, the disastrous effect of seismic pounding may appear between two adjacent unsymmetrical HRBs. For two unsymmetrical L-shape in plan HRBs subjected to earthquake in three different direction cases (*x*, *y,* or both), including the SSI effect, different methods are investigated to mitigate the seismic pounding and thus protect these types of structures under the earthquake effect. The most effective technique to mitigate the seismic pounding and help in seismically protecting these adjacent HRBs is found herein to be the use of a combination of pounding tuned mass dampers (PTMDs) all over the height (at the connection points) together with tuned mass dampers (TMDs) on the top of both buildings.

Keywords: building vibration control; finite element method (FEM); high-rise building (HRB); irregular building; L-shape in plan building; nonlinear time history analysis; pounding tuned mass damper (PTMD); soil-structure interaction (SSI); tuned mass damper (TMD); unsymmetrical in plan building

1. Introduction

This research considers the conditions of utilization and architectural requirements that influence the shape of a building's horizontal plane. The structural engineer plays a crucial role in designing structures capable of withstanding natural disasters, such as earthquakes. Among the challenges faced is the phenomenon known as pounding, which occurs when adjacent buildings experience lateral forces from earthquakes. Additionally, unsymmetrical in-plan shapes, particularly L-shapes, exacerbate and complexities associated with the pounding.

Previous studies have shed light on various aspects of pounding and potential mitigation

*Corresponding author, Professor, E-mail: farghaly@techedu.sohag.edu.eg
**Co-corresponding author, Associate Professor, E-mail: kontoni@uop.gr

http://www.techno-press.org/?journal=csm&subpage=8 ISSN: 2234-2184 (Print), 2234-2192 (Online)

measures. For instance, Abd-El-Rahim and Farghaly (2010) highlighted the sensitivity of induced base shear perpendicular to the earthquake direction to torsional eccentricity, with varying percentages for T, L, and U-shaped buildings. Farghaly (2017) explored the effectiveness of Tuned Mass Dampers (TMDs) in mitigating the impact of earthquakes on L-shaped irregular buildings. Lin *et al.* (2017) conducted shaking table tests, demonstrating the superior control effectiveness of Pounding Tuned Mass Dampers (PTMDs) over traditional TMDs in reducing straining actions during pounding.

Pounding also affects the structural response and inelastic demands of lower floors, particularly in non-aligned adjacent structures, as highlighted by Skrekas *et al.* (2014). The arbitrary direction of earthquake excitation and its influence on pounding effects were emphasized by Polycarpou *et al.* (2015). Lin *et al.* (2016) further investigated the control efficiency of PTMDs, including the use of multiple PTMDs, under severe excitations.

Numerical studies conducted by Bi *et al.* (2017) examined pounding between asymmetric buildings, taking into account arbitrary 3D pounding locations. Kheyroddin *et al.* (2018) explored the impact of adjacent building structural systems on the pounding forces experienced by different building types. Similarly, Abdel Raheem *et al.* (2019) analyzed the effects of seismic pounding parameters, including vibrations, ground motions, building positions, and earthquake angles.

Further investigations by Kontoni and Farghaly (2018, 2019a, b, 2020, 2023) and Farghaly and Kontoni (2022) addressed double pounding, soil-structure interaction, and the effectiveness of various vibration control systems in mitigating seismic responses in different building and structure types.

Zhang and Li (2021) experimentally and numerically analyzed the behavior of L-shaped RC walls under unsymmetrical bending, considering out-of-plane reaction forces and cracking effects. Abdel Raheem *et al.* (2021) studied the impact of structure-soil-structure interaction (SSSI) on the seismic pounding of adjacent buildings, particularly in terms of story displacement, moment, and shear responses.

Jaradat and Far (2021) highlighted the significance of impact spring element stiffness in the pounding analysis of adjacent buildings subjected to earthquakes, with the number of impacts and maximum impact force being crucial parameters.

In this research, the focus is on analyzing two adjacent 3D unsymmetrical L-shaped (in plan) high-rise buildings (of 15 stories) considering soil-structure interaction (SSI) and subjected to earthquake in various directions (*x*, *y*, or both). Time history analyses are conducted to investigate the most effective mitigation system. The combination of PTMDs and TMDs is utilized to achieve optimal seismic response results for these systems.

2. Model description

The problem of unsymmetrical buildings for operational utilities is a complicated problem for civil engineering, especially when the seismic analysis for these buildings is performed taking into consideration the effect of soil-structure interaction. To search for ways to mitigate the effects of the collision between buildings that are not symmetrical in the horizontal plane, the model most affected by earthquakes in both displacements and internal forces was chosen, which is the plan in the form of an L-shape, as well as it was affected by the different earthquake directions to develop a strategy that can mitigate the seismic effect. The effect of earthquakes on the structure and the protection of the two adjacent buildings from the danger of collision, taking into account the effect

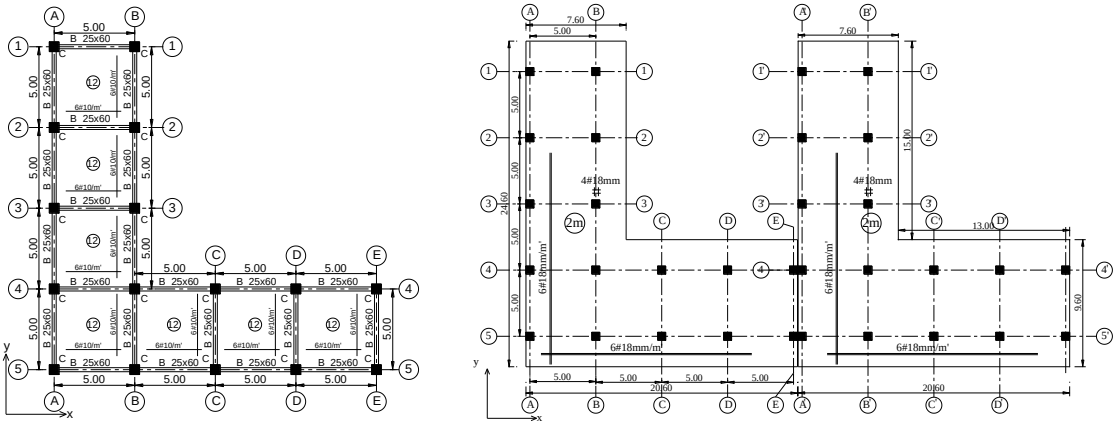

(i) Structural plan (ii) Foundation system of the two buildings (raft)

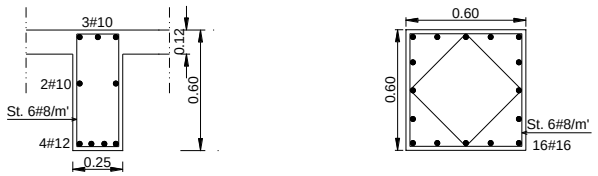

(a) Beam reinforcements (b) Column reinforcements

(iii) Beam and column structural details

Fig. 1 Structural details of the model

of the soil on which the buildings are founded. Fig. 1 shows the structural details of the two similar in the plan and in the foundation system HRBs of 15 floors in height from the ground level, of 3 m for each floor. The beams and columns were represented as frame elements (flexural elements), and slabs and foundations as shell elements. Fig. 1(i) represents the structural plan of the repeated floor for the two buildings.

Fig. 1(ii) shows the structural details of the foundation system of the two adjacent buildings as a flat slab with a thickness of 2 m and two reinforcements nets (up and down) 6#18 mm/m' in both directions (x, and y directions) with additional reinforcements 4#18 mm at the positions of the columns. The irregularity of the L-shaped foundations affects the structural system in two ways: the first way is the effect on the distribution of the soil stress under the foundations such that the stress of soil increases in the connecting line between the two buildings and decreases in the far sides of the buildings, the second way is the possibility of damaging in the foundations if pounding happens at foundation level too.

The details of the structural elements are shown in the structural plan, and the structural details of the beam and column are explained in Fig. 1(iii). The soil under the raft foundation of the two adjacent buildings is medium soil, representing its behavior in the SAP2000 model as gap elements with spring stiffness (k) and dashpot damping (d). Table 1 represents the properties of the used material in each building.

Material nonlinearity and geometric nonlinearity due to the P-Delta effect are considered in the analysis. Contact between the buildings is modeled using 20 mm length elements as contact elements with uni-axial material properties. A value of k_I=93500 kN/m used by Jankowski (2005) for concrete-to-concrete impact is also used in this study. The coefficient of restitution is taken to

Table 1 Properties of the used material in each building (concrete and reinforcement steel)

Property	Value
Compressive strength (f'_c) (MPa)	38.1
Splitting tensile strength (f'_{ct}) (MPa)	3.4
Modulus of rupture (f_r) (MPa)	3.75
Modulus of elasticity (E_c) (MPa)	22938.5
Properties of steel reinforcement material	
Yield stress (f_y) (MPa)	578.18
Ultimate stress (f_u) (MPa)	655.74

Table 2 Properties of the used soil (medium soil)

Properties	Soil
Specific gravity (G_s)	2.65
Liquid limit %	41.5
Plastic limit %	22.6
Plasticity index %	18.9
Uniformity coefficient	1.46
Coefficient of curvature	1.09
Dry density (g/cm^3)	1.75
E (N/mm^2)	20
v	0.4
G (kPa)	15

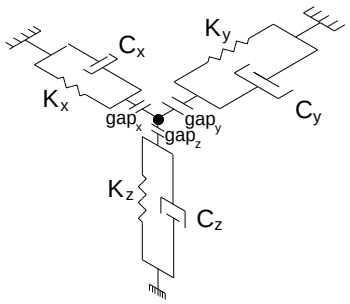

Fig. 2 3D soil element

be 0.65 as used by other researchers for concrete-to-concrete impact (Jankowski 2005, Anagnostopoulos and Karamaneas 2008).

3. Soil-Structure Interaction (SSI)

The properties of the used soil (medium soil) are shown in Table 2. The stiffness and damping parameters of the soil in the vertical and horizontal directions for the 3D soil elements with two gaps in x and y directions to ensure the separation between the soil and the raft foundation when subjected to a lateral force (earthquake loads) as shown in Fig. 2. Table 3 represents the equations

Table 3 Stiffness and damping values for the soil under the raft foundation

Direction	Stiffness	Damping	Mass
Vertical	$k = \frac{4Gr}{1-\nu}$	$1.79\sqrt{k\rho r^3}$	$1.50\rho r^3$
Horizontal	$18.2Gr\frac{1-\nu^2}{2-\nu^3}$	$1.08\sqrt{k\rho r^3}$	$0.28\rho r^3$

G=shear modules, *r*=mass density, *v*=Poisson ratio, *r*=plate radius (Newmark and Rosenblueh 1971)

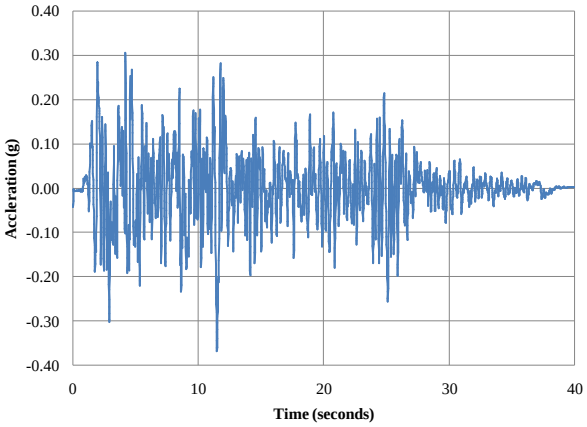

Fig. 3 The El Centro earthquake wave

to calculate the stiffness and damping of soil under raft foundation as per Newmark and Rosenblueth (1971).

4. Earthquake specification

A time history, as shown in Fig. 3, consistent with the 1940 El Centro Earthquake is used in this study. The El Centro earthquake was produced by the strike-slip Imperial fault in the Southern California region. It had a magnitude of 6.9 on the Richter scale and an epicentral distance of 13 km.

Fig. 4 shows the directions of the earthquake in the different states of the buildings. Fig. 4(a) shows the earthquake directions on one building and Fig. 4(b) represents the earthquake directions and the tested points in the two adjacent buildings models to show the lateral displacements in *x* and *y* directions for the single building and the two adjacent buildings.

5. Contact elements

A contact element model represents for the seismic pounding between multi-story buildings (Pant *et al.* 2010, Pant *et al.* 2010), as shown in Fig. 5. The Kelvin-Voigt model is the fundamental linear contact element model, which can take into account the energy dissipated during impact. The gap element in SAP2000 modeling is carried out by providing gap elements (contact

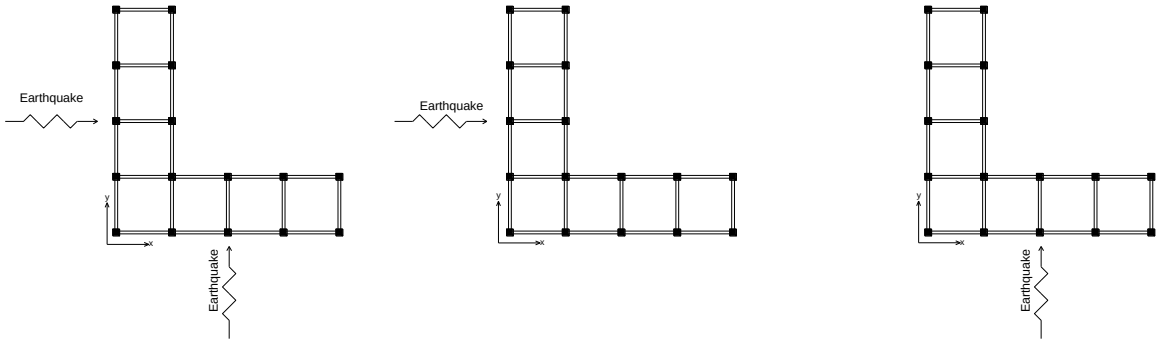

(i) Bidirectional (ii) X-direction (iii) Y-direction

(a) One building

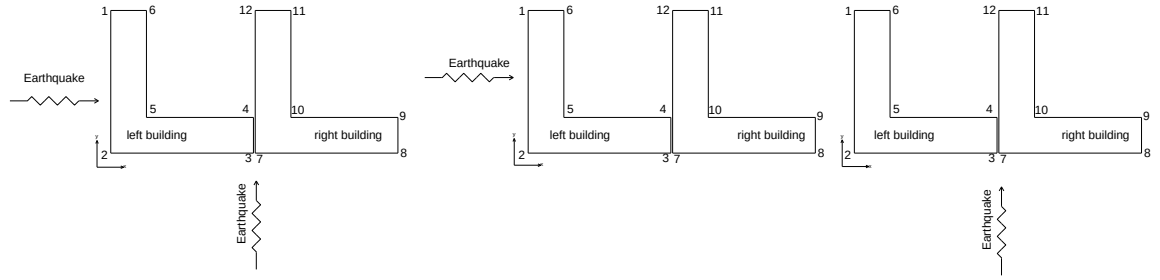

(i) Bidirectional (ii) X-direction (iii) Y-direction

(b) Two adjacent buildings and the tested points

Fig. 4 Earthquake directions

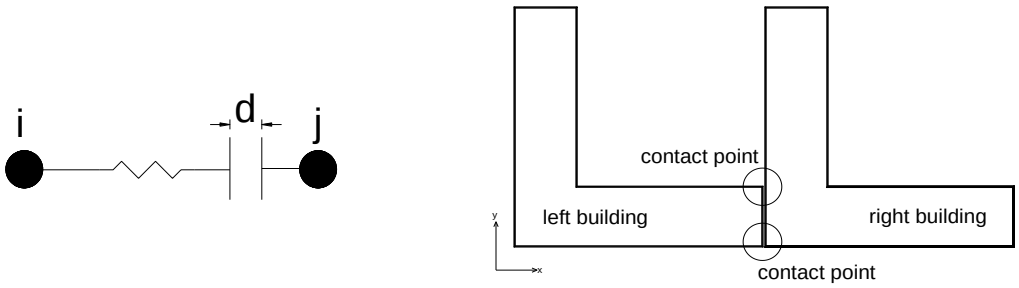

(a) Gap element (b) Position of contact elements at contact points.

Fig. 5 Contact elements

elements) in between the buildings. The gap element gets activated when the net displacement of the building exceeds the gap opening, leading to the generation of collision force. The gap element (of SAP2000) is shown in Fig. 5(a), where *i* and *j* represent the collision point of the left and right building, respectively, *d* represents the opening provided for this pounding study (*d*=20 mm).

The contact (gap) elements are placed at each beam-column connection at the contact area of the two adjacent buildings all over the height of the two buildings (at each floor level) including the foundation level, as shown in Fig. 5(b).

When pounding tuned mass dampers (PTMDs) are used, they are placed instead of the contact

elements in the same positions.

Collisions between the two adjacent buildings can occur at anywhere along the height of the two buildings, including their foundations, and not only at their top. Connecting also the foundations of two adjacent buildings can have several effects on their seismic response. Here are a few potential impacts: increased stiffness and strength, reduced relative movement, transfer of seismic forces, compatibility and design challenges, induced load redistribution, damping and energy dissipation, resonance and amplification, etc. It is important to note that the specific effects of connecting the foundations of adjacent buildings on the seismic response can vary depending on various factors, including the structural characteristics of the buildings, the design of the connection, and the seismicity of the region. Proper engineering analysis and design are crucial to ensure the desired performance and safety of the interconnected buildings during seismic events.

The contact elements which are used in the connections between the two HRBs were extracted from the relation derived by Anagnostopoulos (2004). If the masses m_1 and m_2 are the masses of the two pounding buildings, then the damping c of the impact element in terms of the coefficient of restitution r, as the following Eq. (1)

$$c = 2\zeta\sqrt{\left(k\frac{m_1 m_2}{m_1+m_2}\right)}$$
$$\zeta_i = \frac{\ln r}{\sqrt{[\pi^2 + (\ln r)^2]}} \tag{1}$$

where k is the stiffness of the impact spring, ln$r$ is the natural logarithm of r, and ζ is the damping coefficient. The values of the restitution r are calculated as follows: If considering an elastic impact between the two buildings the value of restitution (r) equals one and damping coefficient (ζ) equals zero, and if considering plastic impact between the two buildings the value of restitution (r) equals zero and damping coefficient (ζ) equals one. The used values in this research are 0.65 and 0.14 for r and ζ, respectively.

6. TMD parameters

For the case when the structure is subjected to a harmonic base excitation, the corresponding expressions can be found to be in Eq. (2) (Zahrai and Ghannadi-Asl 2008)

$$\alpha_{opt.} = \frac{1}{1+\mu}\sqrt{\frac{2-\mu}{2}}$$
$$\zeta_{opt.} = \sqrt{\frac{3\mu}{8(1+\mu)}}.\sqrt{\frac{2}{2-\mu}} \tag{2}$$
$$k_d = 4\pi^2\mu\alpha^2\frac{m_s}{T_s^2}$$
$$c_d = 4\pi\mu\alpha\zeta_{opt.}\frac{m_s}{T_s}$$

In the presence of damping for the main mass, no closed-form expressions can be derived for

Table 4 The dynamic properties of the PTMD

	Fundamental natural frequency (Hz)	Stiffness (N/m)	Mass (kg)	Damping ratio	Mass ratio
PTMD	1.20	42.20	0.746	0.29%	0.0593

the optimum damper parameters. However, they may be obtained by numerical trials with the aim of achieving a system with the smallest possible value of its higher response peak.

7. PTMD properties

As expressed by Xue *et. al.* (2016), the properties of the viscoelastic material layer in PTMD will give different vibration reduction results. Material with a higher equivalent elasticity modulus can induce a larger pounding force under the same situation, which may enhance the controlling force and get more momentum exchanged during an impact. Tuning to the natural frequency of the primary structure is the most important purpose of traditional TMD design. However, it is difficult to measure the natural frequency of the structure accurately. To quantify the degree of deviation between an optimal frequency and tuned frequency in TMD and PTMD, the detuning ratio (DTR) is defined as follows:

$$DTR = \frac{f_{damper} - f_{opt}}{f_{opt}} . 100\% \quad (3)$$

where f_{damper} is the frequency of the PTMD or TMD and f_{opt} is the optimal frequency.

As a comparison shown by Xue *et al.* (2016), the control performance of the TMD with the same detuning ratio is nearly three times as much as PTMD under 0.74 Hz and four times of a 1.00 Hz TMD; that simulation result demonstrated that PTMD can suppress the vibration and dissipate energy more effectively and show excellent adaptability and strong robustness. From an energy viewpoint, energy can be dissipated from the damper in TMD or PTMD, as well as the impact process between the mass block and viscoelastic material. A small gap in PTMD means that the mass will impact the viscoelastic material more severely and frequently. In an extreme case where the gap is large enough, the impact will not happen, and PTMD turns into a traditional TMD. The dynamic properties of the proposed PTMD are shown in Table 4.

8. Results and discussion

Two 3D models with 15 floors and an L-shape plan were studied to show the effect of seismic pounding between the two building models with soil-structure interaction (the two models were founded on raft foundation) subjected to an earthquake (El Centro) and study the mitigation system which controls the response of the effect of the earthquake. For comparison reasons, the model was subjected to the earthquake without any control system, and the results were compared with the chosen systems to show its efficiency in resisting the earthquake effect, including the effect of SSI.

Herein the maximum time history values are presented.

Fig. 6(a) shows the top lateral displacements in the *x*-direction for the single and the two adjacent buildings subjected to the El Centro earthquake in different directions (*x*- or *y*-direction,

or both directions). Fig. 6(a(i)) shows the lateral displacements in the *x*-direction of the single and two adjacent buildings subjected to *x*-direction earthquake, where the six points of each model showed that the biggest lateral displacements occurred in two adjacent buildings than in the single building. Fig. 6(a(ii)) represents the lateral displacements in the *x*-direction for the points of the two models subjected to *y*-direction earthquake, where the two adjacent buildings recorded higher values than the corresponding values in the single model. Fig. 6(a(iii)) represents the lateral displacements in the *x*-direction for the two buildings model subjected to bidirectional earthquake (*x*-and *y*- direction earthquake), where the top points of the two adjacent buildings recorded the highest values of lateral displacements than the single model, and this is due to the collision between the two adjacent buildings and the twisting of each building separately.

Fig. 6(b) shows the top lateral displacements in the *y*-direction for the single and the two adjacent buildings subjected to the El Centro earthquake in different directions (*x*- or *y*-direction, or both directions). Fig. 6(b(i)) shows the lateral displacements in the *y*-direction of the single and two adjacent buildings subjected to *x*-direction earthquake, where the six points of each model showed that the biggest lateral displacements occurred in two adjacent buildings than in the single building. Fig. 6(b(ii)) represents the lateral displacements in the *y*-direction for the points of the two models subjected to *y*-direction earthquake, where the two adjacent buildings recorded higher values than the corresponding values in the single model. Fig. 6(b(iii)) represents the lateral displacements in *y*-direction for the two buildings model subjected to bidirectional earthquake (*x*- and *y*- direction earthquake), where the top points of the two adjacent buildings recorded the highest values of lateral displacements than the single model, and this is due to the collision between the two adjacent buildings and the twisting of each building separately.

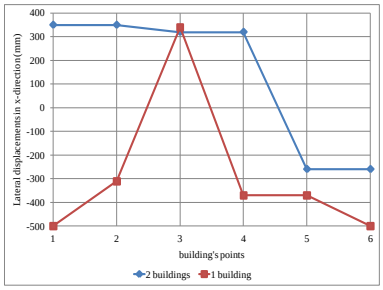

(i) Earthquake in *x*-direction

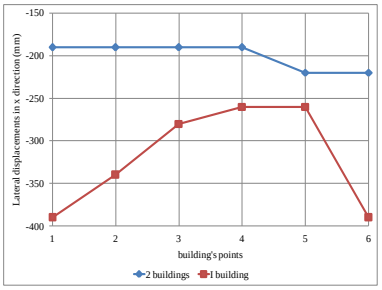

(ii) Earthquake in *y*-direction

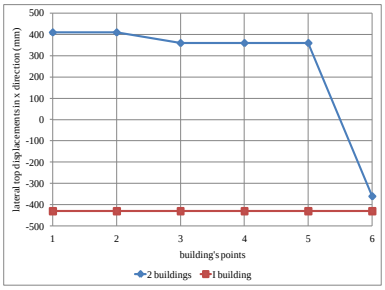

(iii) Bidirectional earthquake

(a) *X*-direction

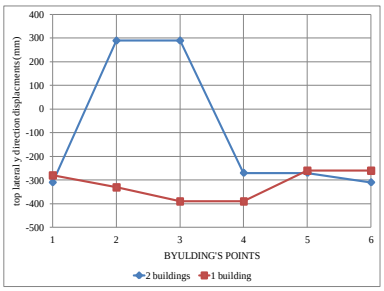

(i) Earthquake in *x*-direction

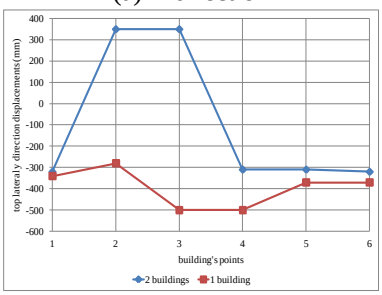

(ii) Earthquake in *y*-direction

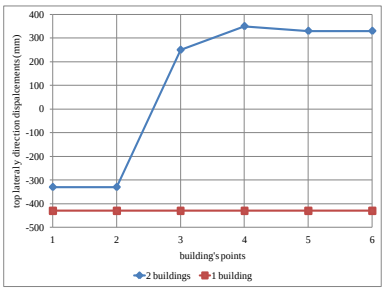

(iii) Bidirectional earthquake

(b) *Y*-direction

Fig. 6 Top lateral displacements

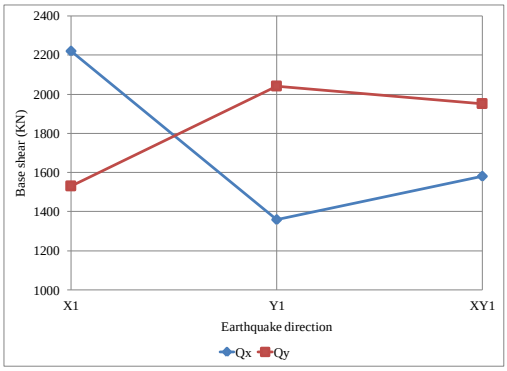

(i) Single building

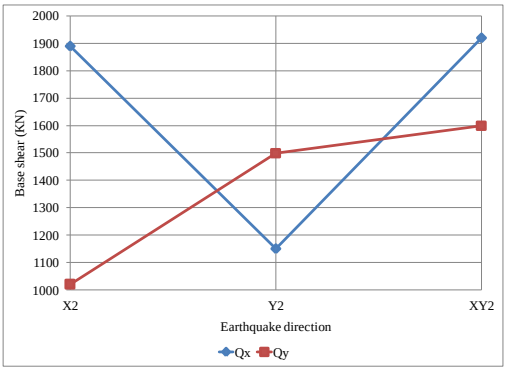

(ii) One of the two adjacent buildings

(a) Base shears

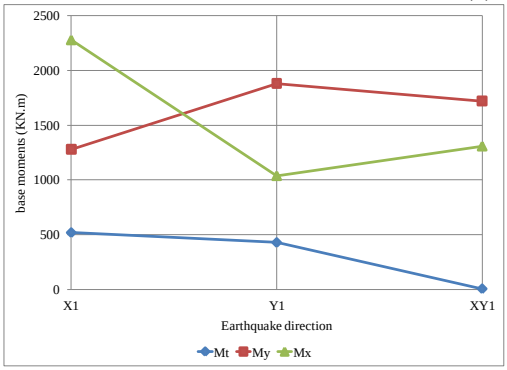

(i) Single building

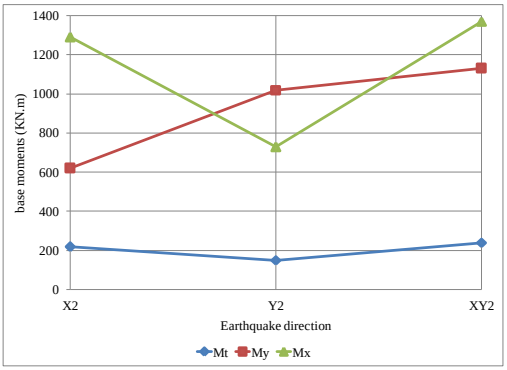

(ii) One of the two adjacent buildings

(b) Base moments

Fig. 7 Base straining actions

Fig. 7(a) shows the base shears in *x* and *y* directions (Q_x and Q_y) for the two models (single and two adjacent buildings), subjected to different direction earthquakes. Fig. 7(a(i)) represents the base shear for the single building subjected to *x*- or *y*-direction, or both directions earthquakes. When the model is exposed to the seismic wave in a certain direction, the base shear does not appear only in this direction, but appears to have also a value in the direction perpendicular to the direction of the effect of the earthquakes, and this is a result of the irregularity of the horizontal plane of the model even so these values are small, the ratio between the values and the perpendicular ones is nearly about 1.40. Fig. 7(a(ii)) represents the base shear for one building of the two adjacent buildings subjected to *x*- or *y*-direction, or both directions earthquakes. When the model is exposed to the seismic wave in a certain direction, but with smaller values than the single model case, the base shear does not appear only in this direction, but appears to have also a value in the direction perpendicular to the direction of the effect of the earthquakes, and this is a result of the irregularity of the horizontal plane of the model even so these values are small, the ratio between the values and the perpendicular ones nearly about 1.30; but at the *x*-direction earthquake, the base shear ratio between *x* and *y* directions base shears is nearly 1.90 which is bigger than single building case, and this is due to the fact that the collision between the two buildings led to an increase in the base shear.

Fig. 7(b) represents the base moments in *x*, *y*, and *z* directions (M_x, M_y, and Torsion M_t) of the two models subjected to earthquake in different directions. Fig. 7(b(i)) represents the base moments for the single building subjected to *x*- or *y*-direction, or both directions earthquakes. When the model is exposed to the seismic wave in a certain direction, the base moment does not appear only in this direction, but appears to have also a value in the direction perpendicular to the direction of the effect of the earthquake, and this is a result of the irregularity of the horizontal plane of the model even so these values are small, the ratio between the values and the perpendicular nearly about 1.80. The base torsion for the building recorded constant values for each earthquake direction except the bidirectional earthquake direction (nearly equals zero). Fig. 7(b(ii)) represents the base moments for one building of the two adjacent buildings subjected to *x*- or *y*-direction, or both directions earthquakes. When the model is exposed to the seismic wave in a certain direction, but with small values than the single model case, the moment does not appear only in this direction, but appears to have also a value in the direction perpendicular to the direction of the effect of the earthquakes, and this is a result of the irregularity of the horizontal plane of the model even so these values are small, the ratio between the values and the perpendicular nearly about 1.3; but at the *x*-direction earthquake, the base shear ratio between *x* and *y* directions base shears is nearly 2.2 which is bigger than single building case, and this is due to the fact that the collision between the two buildings led to an increase in the base moment. The base torsion for the building recorded constant values for each earthquake direction.

Deformations occurring in the horizontal plane of the building, whether for the single building or the two adjacent buildings as a result of earthquakes of different directions, as well as the increase in internal forces, whether the base shear or the base moments as a result of the collision of the two adjacent buildings due to earthquakes using top TMDs, or PTMD or a combination of them. Three strategies were used to reduce the harmful effect of the earthquake and the irregularity of the plan, top TMDs, or PTMD, or a combination of them. Table 5 represents the abbreviations and symbols' meanings used in this paper.

Table 5 The abbreviations and symbols' meanings

Symbol	Meaning
1TMD	Six top TMDs on the left building.
2TMD	Six top TMDs on each left and right buildings.
PTMD	Pounding tuned mass damper (PTMD).
GAP	Gap elements between the two adjacent buildings all over the height of the two buildings.
1, 2, …., 6	Top left building points.
7, 8, …., 12	Top right building points.
Case 1	(2TMD+GAP): Mitigation technique using top corners TMDs on both two adjacent buildings.
Case 2	(1TMD+GAP): Mitigation technique using top corners TMDs on the left building.
Case 3	(PTMD): Mitigation technique using PTMD between the two adjacent buildings all over the height at the contact area between the two adjacent buildings.
Case 4	(PTMD+2TMD): Mitigation technique using PTMD between the two adjacent buildings all over the height at the contact area between the two adjacent buildings and top corners TMDs on both two adjacent buildings.
Case 5	(PTMD+1TMD): Mitigation technique using PTMD between the two adjacent buildings all over the height at the contact area between the two adjacent buildings and top corners TMDs on left building.

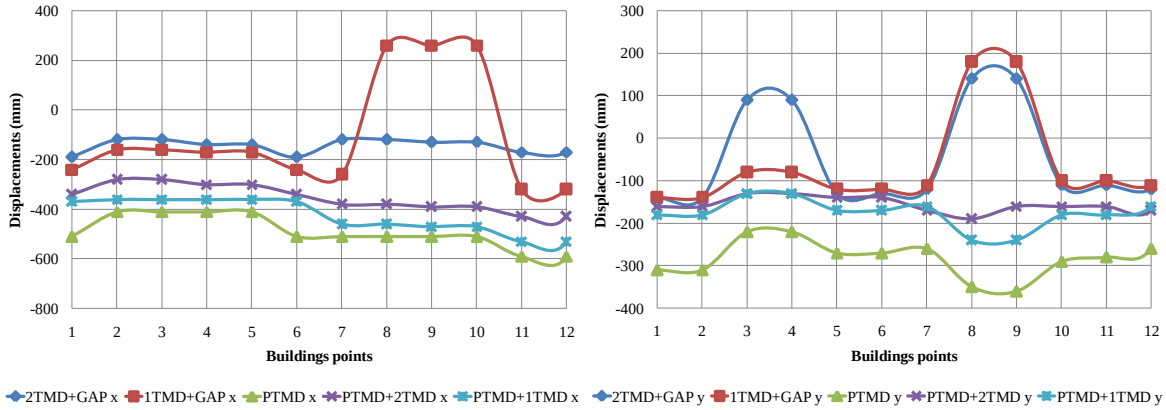

(i) Lateral *x* displacements (ii) Lateral *y* displacements

Fig. 8 Top lateral displacements for different mitigation methods

Fig. 8 represents the top lateral displacements in the *x* and *y* directions of the two adjacent buildings subjected to *x*-direction earthquake with different kinds of mitigation systems. Fig. 8(i) shows the lateral displacements in the *x*-direction of the top corners points of the two adjacent buildings (points 1 to 6 for the left building, and points 7 to 12 for the right building), the right building was affected by pounding at points 8, 9, and 10 with top TMDs on the left building. Fig. 8(ii) shows the lateral displacements in the *y*-direction of the top corners points of the two adjacent buildings, the left and right buildings were affected by pounding at points 3 and 4 (left building), and points 8 and 9 (right building) with top TMDs on the right and left buildings and TMDs on top of the right building only respectively. The most steady cases appear at using PTMD all over the height of the two adjacent buildings for the use of only PTMD or for a combination of PTMD with one top TMDs building or two buildings top TMDs, but the GAP with TMDs over one or two buildings recorded high lateral displacements for both buildings.

Fig. 9(a) shows the base shears in *x* and *y* directions for the two adjacent buildings subjected to one direction earthquake (in the *x*-direction) computed with five mitigation methods (cases 1 to 5) to show which is the appropriate method to reduce the earthquake effect. Fig. 9(a(i)) shows the base shears in *x* and *y* directions for the left building, where the maximum base shear appears in case 3 (PTMD), and the minimum base shear appears in case 4 (PTMD+2TMDs). Fig. 9(a(ii)) shows the base shears in *x* and *y* directions for the right building, where the maximum base shear appears in case 3 (PTMD), and the minimum base shear appears in case 4 (PTMD+2TMDs).

Fig. 9(b) shows the base moments in *x*, *y* and *z* directions (M_x, M_y, Torsion M_t) for the two adjacent buildings subjected to one direction earthquake (in the *x*-direction) computed with five mitigation methods (cases 1 to 5) to show which is the appropriate method to reduce the earthquake effect. Fig. 9(b(i)) shows the base moments in *x*, *y* and *z* directions for the left building, where the maximum base moments appear in case 3 (PTMD), and the minimum base moments appear in case 4 (PTMD+2TMDs). Fig. 9(b(ii)) shows the base moments in *x*, *y* and *z* directions for the right building, where the maximum base moments appear in case 3 (PTMD) and the minimum base moments appear in case 4 (PTMD+2TMDs).

Fig. 10 represents the lateral displacements in the *x* and *y* directions of the two adjacent buildings subjected to *y*-direction earthquake with different kinds of mitigation systems. Fig. 10(i) shows the lateral displacements in the *x*-direction of the top corners points of the two adjacent

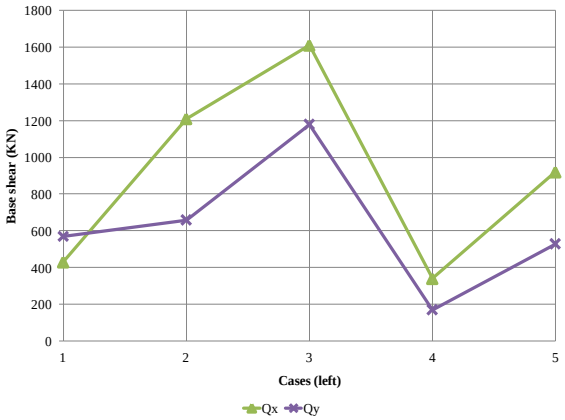

(i) Left building

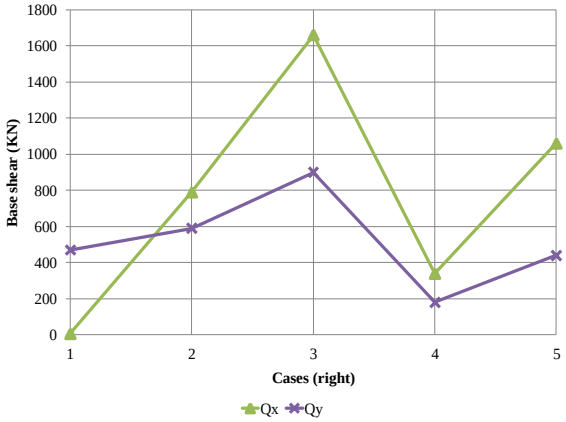

(ii) Right building

(a) Base shears for *x*-direction earthquake

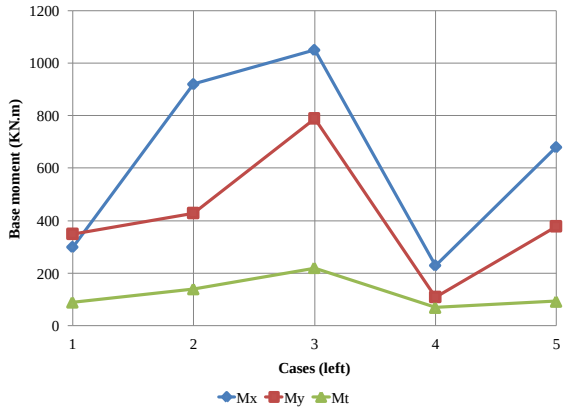

(i) Left building

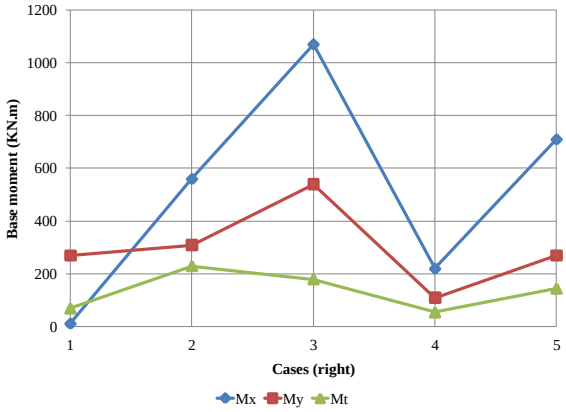

(ii) Right building

(b) Base moments for *x*-direction earthquake

Fig. 9 Base straining actions

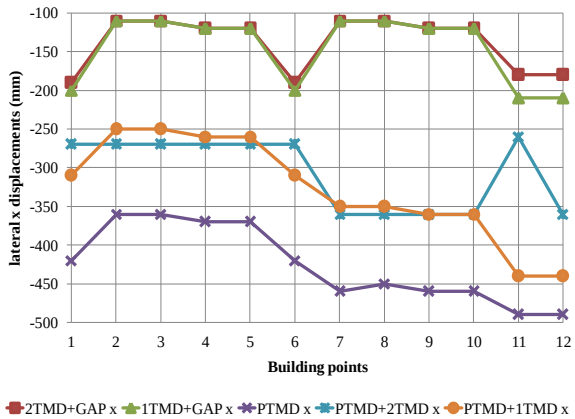

(i) Lateral *x* displacements

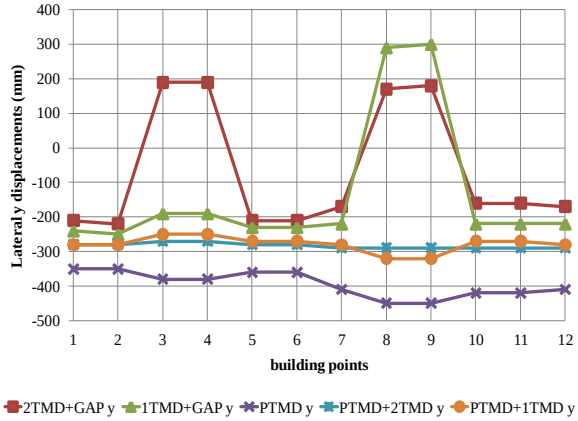

(ii) Lateral *y* displacements

Fig. 10 Lateral displacements for *y*-direction earthquake

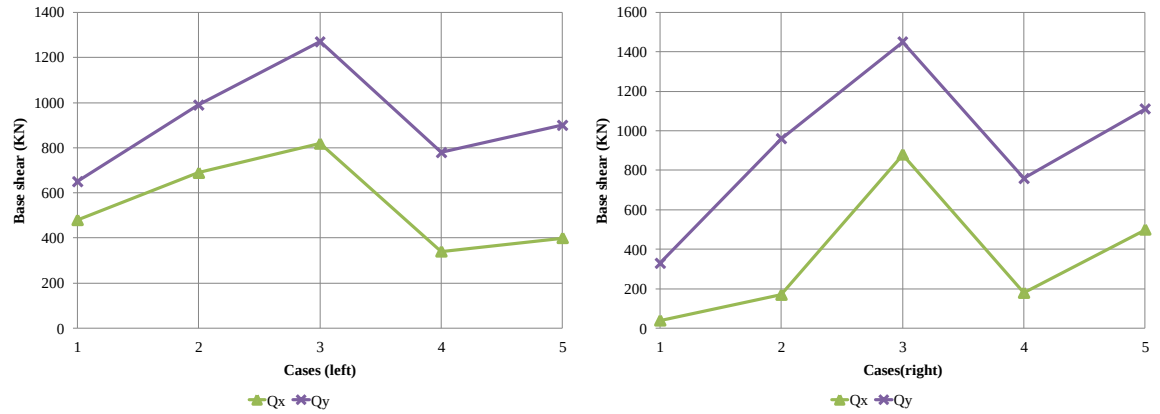

(i) Left building (ii) Right building

(a) Base shears

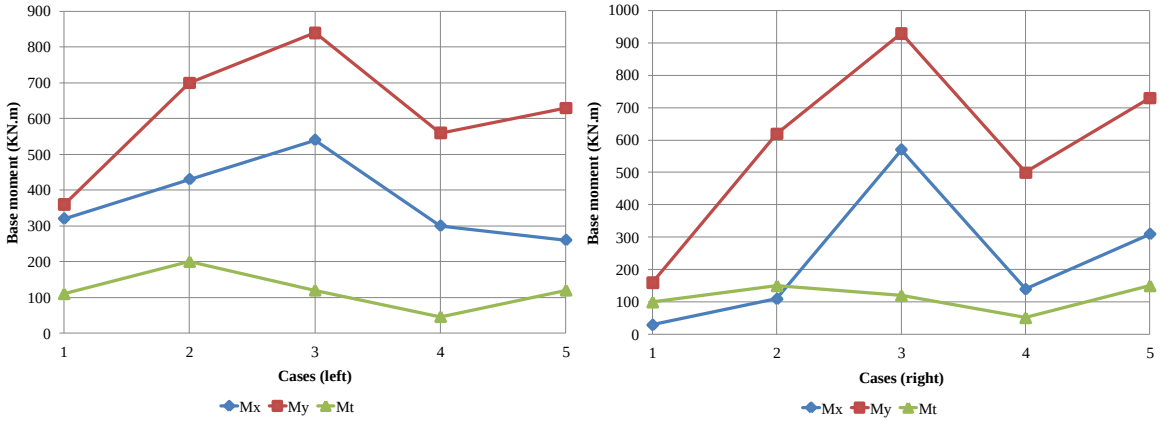

(i) Left building (ii) Right building

(b) Base moments

Fig. 11 Base straining actions in the *y* direction

buildings (points 1 to 6 for the left building, and points 7 to 12 for the right building), where the minimum top displacements for the two adjacent buildings were recorded in the cases 1 and 2, and the maximum displacements were recorded in case 3 (PTMD). Fig. 10(ii) shows the lateral displacements in the *y*-direction of the top corners points of the two adjacent buildings, where the left and right buildings were affected by pounding at points 3 and 4 (left building) and points 8 and 9 (right building) with top TMDs on the right and left buildings and TMDs on top of the right building only, respectively. The most steady cases appear when using PTMD all over the height of the two adjacent buildings for the use of only PTMD or for the combination of PTMD with one top TMDs building or two buildings with top TMDs, but the GAP with TMDs over one or two buildings recorded high lateral displacements for both buildings.

Fig. 11 shows the base shears in *x* and *y* directions for the two adjacent buildings subjected to one direction earthquake (in the *y*-direction) computed with five mitigation methods (cases 1 to 5) to show the most appropriate method to reduce the earthquake effect. Fig. 11(a(i)) shows the base shears in *x* and *y* directions for the left building, where the maximum base shear appears in case 3

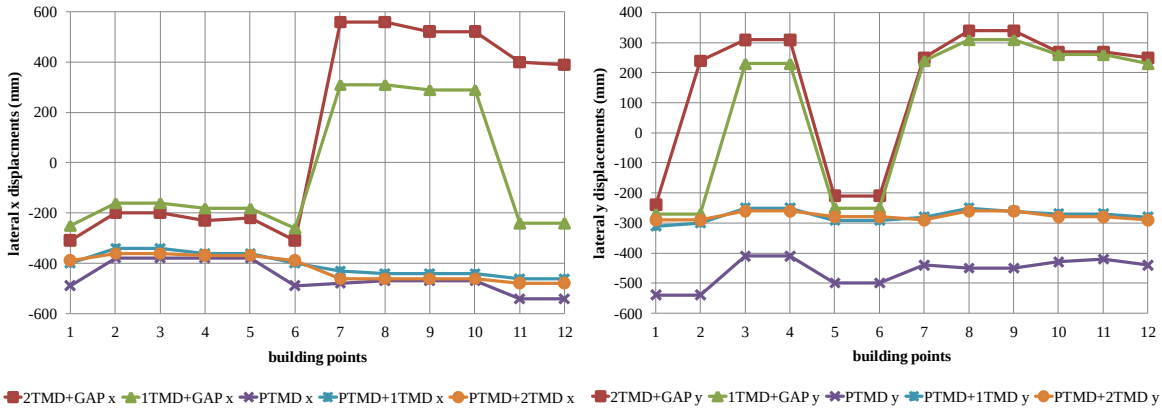

(i) Lateral *x* displacements (ii) Lateral *y* displacements

Fig. 12 Top lateral displacements for bidirectional earthquake

(PTMD), and the minimum base shear appears in case 4 (PTMD+2TMDs). Fig. 11(a(ii)) shows the base shears in *x* and *y* directions for the right building, where the maximum base shear appears in case 3 (PTMD), and the minimum base shear appears in case 4 (PTMD+2TMDs). Fig. 11(b) shows the base moments in *x*, *y* and *z* directions (M_x, M_y, Torsion M_t) for the two adjacent buildings subjected to one direction earthquake (in the *y*-direction) prepared with five mitigation methods (cases 1 to 5) to show what the appropriate method to reduce the earthquake effect. Fig. 11(b(i)) shows the base moments in *x*, *y* and *z* directions (M_x, M_y, Torsion M_t) for the left building, where the maximum base moments appear in case 3 (PTMD), and the minimum base moments appear in case 4 (PTMD+2TMDs). Fig. 11(b(ii)) shows the base moments in *x*, *y* and *z* directions (M_x, M_y, Torsion M_t) for the right building, where the maximum base moments appear in case 3 (PTMD), and the minimum base moments appear in case 4 (PTMD+2TMDs) and case 1 (2TMDs+GAP).

Fig. 12 shows the lateral displacements in *x* and *y* directions for the two adjacent buildings subjected to bidirectional (*x*- and *y*-directions) earthquake with different kinds of mitigation systems. Fig. 12(i) shows the lateral displacements in the *x*-direction of the top corners points of the two adjacent buildings, the minimum top displacements for the two adjacent buildings were recorded in cases 1 and 2, and the maximum displacements were recorded in case 3 (PTMD). Fig. 12(ii) shows the lateral displacements in the *y*-direction of the top corners points of the two adjacent buildings, where the left and right buildings were affected by pounding at points 3 and 4 (left building), and points 8 and 9 (right building) with top TMDs on the right and left buildings and TMDs on top of the right building only, respectively. The most steady cases appear when using PTMD all over the height of the two adjacent buildings for the use of only PTMD or for the combination of PTMD with one top TMDs building or two buildings with top TMDs, but the GAP with TMDs over one or two buildings recorded high lateral displacements for both buildings.

Fig. 13 shows the base shears in the *x* and *y* direction for the two adjacent buildings subjected to bidirectional (*x*- and *y*-directions) earthquake computed with five mitigation methods (cases 1 to 5) to show which is the appropriate method to reduce the earthquake effect. Fig. 13(i) shows the base shears in the *x* and *y* directions for the left building, where the maximum base shear appears in case 3 (PTMD), and the minimum base shear appears in case 4 (PTMD+2TMDs). Fig. 13(ii) shows the base shears in the *x* and *y* directions for the right building, where the maximum base

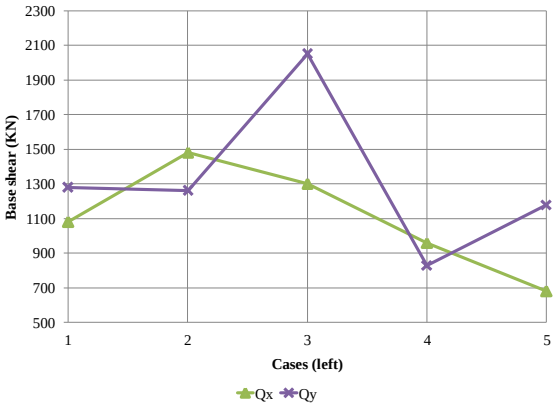

(i) Left building

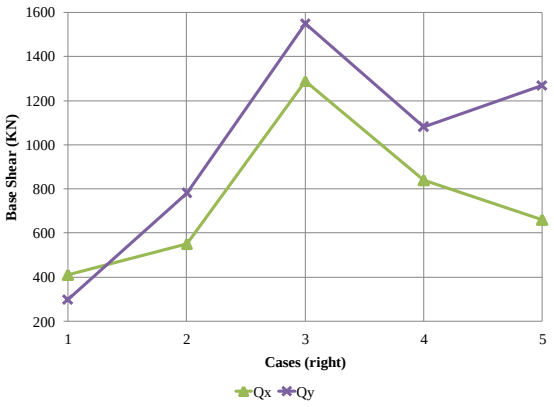

(ii) Right building

Fig. 13 Base shears for bidirectional earthquake

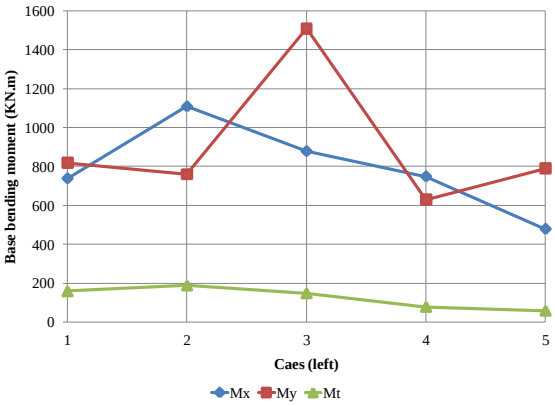

(i) Left building

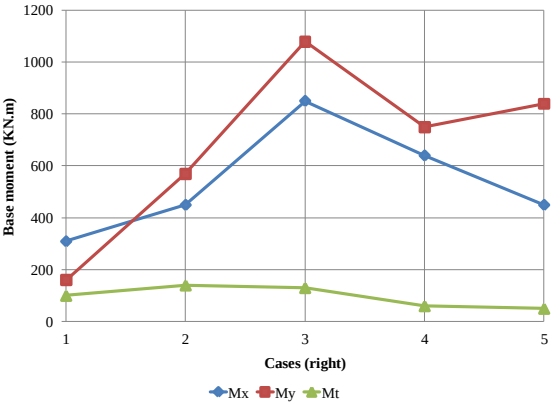

(ii) Right building

Fig. 14 Base moments for bidirectional earthquake

shear appears in case 3 (PTMD), and the minimum base shear appears in case 1 (2TMDs+GAP).

Fig. 14 shows the base moments in *x*-, *y*- and *z*-direction (M_x, M_y, Torsion M_t) for the two adjacent buildings subjected to bidirectional (*x*- and *y*-directions) earthquake computed with five mitigation methods (cases 1 to 5) to show which the appropriate method to reduce the earthquake effect. Fig. 14(i) shows the base moments in *x*, *y* and *z* directions for the left building, where the maximum base moments appear in case 3 (PTMD), and the minimum base moments appear in case 4 (PTMD+2TMDs). Fig. 14(ii) shows the base moments in *x*, *y* and *z* directions for the right building, where the maximum base moments appear in case 3 (PTMD), and the minimum base moments appear in case 1 (2TMDs+GAP).

9. Conclusions

Two 3D L-shape in plan adjacent high-rise buildings subjected to three earthquake direction cases with the same earthquake wave (El Centro earthquake) in the *x*-direction, in the *y*-direction,

and in both *x* and *y* directions on both buildings to show the extremes effect of earthquake on each building. Five mitigation techniques were used for the special treatment of such special adjacent buildings with special earthquake effects of them, top corners TMDs on both adjacent buildings with a gap between the two adjacent buildings, top corners left building with a gap between the two adjacent buildings, pounding tuned mass dampers between the two adjacent buildings, pounding tuned mass dampers between the two adjacent buildings with top corners TMDs on the two adjacent buildings, and pounding tuned mass dampers between the two adjacent buildings with top corners TMDs on the left building, the parameters were checked top lateral displacements in *x* and *y* directions, base shear in *x* and *y* directions and base moments in *x*, *y*, and *z* directions, from the previous results the concluding remakes can be drawn:

- The direction of the earthquake affects the behavior of the irregular structure.
- An irregular in-horizontal-plan building exposed to earthquakes leads to a horizontal displacement in addition to the torsion of the building, and this is an additional source of horizontal forces to the adjacent building, which increases the seismic effect on the adjacent irregular-in-plan buildings.
- TMDs affect the lateral displacements, especially if they are equipped on both two adjacent buildings.
- PTMDs work well with the TMDs on the top of both adjacent buildings.
- The base moments develop high values in the case of one direction earthquake (*x*- or *y*-direction) affecting both adjacent buildings.
- The most effective mitigation technique for the adjacent buildings is both TMDs on the top of the two buildings and PTMDs all over the height of the buildings at the connection points.

In future studies, the following points can be investigated:

- Experimental measuring of the stress under the foundations of such buildings.
- Changing the soil type under the foundations of the two buildings (soft and hard soil).
- Changing the type of foundations under the two buildings (use of deep foundations).

References

Abdel Raheem, S.E., Alazrak, T.M.A., AbdelShafy, A.G.A., Ahmed, M.M. and Yasser Gamal, Y.A.S. (2021), "Seismic pounding between adjacent buildings considering soil-structure interaction", *Earthq. Struct.*, **20**(1), 55-70. http://doi.org/10.12989/eas.2021.20.1.055.

Abdel Raheem, S.E., Fooly, M.Y.M., Omar, M. and Abdel Zaher, A.K. (2019), "Seismic pounding effects on the adjacent symmetric buildings with eccentric alignment", *Earthq. Struct.*, **16**(6), 715-726. http://doi.org/10.12989/eas.2019.16.6.715.

Abd-El-Rahim, H.H.A. and Farghaly, A.A. (2010), "Influence of structural irregularity in plan floor shape on seismic response of buildings", *J. Eng. Sci., Assiut Univ.*, **38**(4), 911-928.

Anagnostopoulos, S.A. (2004), "Equivalent viscous damping for modeling inelastic impacts in earthquake pounding problems", *Earthq. Eng. Struct. Dyn.*, **33**(8), 897-902. https://doi.org/10.1002/eqe.377.

Anagnostopoulos, S.A. and Karamaneas, C.E. (2008), "Use of collision shear wall to minimize seismic separation and to protect adjacent buildings from collapse due to earthquake-induced pounding", *Earthq. Eng. Struct. Dyn.*, **37**(12), 1371-1388. https://doi.org/10.1002/eqe.817.

Bi, K., Hao, H. and Sun, Z. (2017), "3D FEM analysis of earthquake induced pounding responses between asymmetric buildings", *Earthq. Struct.*, **13**(4), 377-386. http://doi.org/10.12989/eas.2017.13.4.377.

Farghaly, A.A. (2017), "Self-control of high rise building L-shape in plan considering soil structure interaction", *Couple. Syst. Mech.*, **6**(3), 229-249. https://doi.org/10.12989/csm.2017.6.3.229.

Farghaly, A.A. and Kontoni, D.P.N. (2022), "Mitigation of seismic pounding between RC twin high-rise

buildings with piled raft foundation considering SSI", *Earthq. Struct.*, **22**(6), 625-635. https://doi.org/10.12989/eas.2022.22.6.625.

Jankowski, R. (2005), "Non-linear viscoelastic modelling of earthquake-induced structural pounding", *Earthq. Eng. Struct. Dyn.*, **34**(6), 595-611. https://doi.org/10.1002/eqe.434.

Jaradat, Y. and Far, H. (2021), "Optimum stiffness values for impact element models to determine pounding forces between adjacent buildings", *Struct. Eng. Mech.*, **77**(2), 293-304. http://doi.org/10.12989/sem.2021.77.2.293.

Kheyroddin, A., Kioumarsi, M., Kioumarsi, B. and Faraei, A. (2018), "Effect of lateral structural systems of adjacent buildings on pounding force", *Earthq. Struct.*, **14**(3), 229-239. http://doi.org/10.12989/eas.2018.14.3.229.

Kontoni, D.P.N. and Farghaly, A.A. (2018), "Seismic response of adjacent unequal buildings subjected to double pounding considering soil-structure interaction", *Comput.*, **6**(1), 1-18. https://doi.org/10.3390/computation6010010.

Kontoni, D.P.N. and Farghaly, A.A. (2019a), "Mitigation of the seismic response of a cable-stayed bridge with soil-structure-interaction effect using tuned mass dampers", *Struct. Eng. Mech.*, **69**(6), 699-712. https://doi.org/10.12989/sem.2019.69.6.699.

Kontoni, D.P.N. and Farghaly, A.A. (2019b), "The effect of base isolation and tuned mass dampers on the seismic response of RC high-rise buildings considering soil-structure interaction", *Earthq. Struct.*, **17**(4), 425-434. https://doi.org/10.12989/eas.2019.17.4.425.

Kontoni, D.P.N. and Farghaly, A.A. (2020), "TMD effectiveness for steel high-rise building subjected to wind or earthquake including soil-structure interaction", *Wind Struct.*, **30**(4), 423-432. https://doi.org/10.12989/was.2020.30.4.423.

Kontoni, D.P.N. and Farghaly, A.A. (2023), "Enhancing the earthquake resistance of RC and steel high-rise buildings by bracings, shear walls and TMDs considering SSI", *Asia. J. Civil Eng.*, 1-14. https://doi.org/10.1007/s42107-023-00666-6.

Lin, W., Lin, Y., Song, G. and Li, J. (2016), "Multiple Pounding Tuned Mass Damper (MPTMD) control on benchmark tower subjected to earthquake excitations", *Earthq. Struct.*, **11**(6), 1123-1141. http://doi.org/10.12989/eas.2016.11.6.1123.

Lin, W., Wang, Q., Li, J., Chen, S. and Qi, A. (2017), "Shaking table test of pounding tuned mass damper (PTMD) on a frame structure under earthquake excitation", *Comput. Concrete*, **20**(5), 545-553. http://doi.org/10.12989/cac.2017.20.5.545.

Newmark, N.M. and Rosenblueth, E. (1971), *Fundamentals of Earthquake Engineering*, Prentice-Hall, Englewood Cliffs, New Jersey.

Pant, D.R., Wijeyewickrema, A.C. and Ohmachi, T. (2010), "Three dimensional nonlinear analysis of seismic pounding between multi-story reinforced concrete buildings", *Proceedings of the Seventh International Conference on Urban Earthquake Engineering (7CUEE) and Fifth International Conference on Earthquake Engineering (5ICEE)*, Tokyo.

Polycarpou, P.C., Papaloizou, L., Komodromos, P. and Charmpis, D.C. (2015), "Effect of the seismic excitation angle on the dynamic response of adjacent buildings during pounding", *Earthq. Struct.*, **8**(5), 1127-1146. http://doi.org/10.12989/eas.2015.8.5.1127.

SAP2000® Version 17 (2015), Integrated Software for Structural Analysis and Design, Computers and Structures, Inc., Walnut Creek, New York, USA.

Skrekas, P., Sextos, A. and Giaralis, A. (2014), "Influence of bi-directional seismic pounding on the inelastic demand distribution of three adjacent multi-storey R/C buildings", *Earthq. Struct.*, **6**(1), 71-87. http://doi.org/10.12989/eas.2014.6.1.071.

Xue Q., Zhang, J., He, J. and Zhang, C. (2016), "Control performance and robustness of pounding tuned mass damper for vibration reduction in SDOF structure", *Shock Vib.*, **2016**, Article ID 2596923. https://doi.org/10.1155/2016/8021690.

Zahrai, S.M. and Ghannadi-Asl, A. (2008), "Seismic performance of TMDs in improving the response of MRF buildings", *Scientia Iranica*, **15**(1), 21-33.

Zhang, Z. and Li, B. (2021), "Seismic performance of L-shaped RC walls

sustaining unsymmetrical bending", *Struct. Eng. Mech.*, **78**(3), 269-280. http://doi.org/10.12989/sem.2021.78.3.269.

CC